

Electronic Supplementary Information (ESI)

Evolution From [Zn₉] to Record-High [Zn₅₄] Subblock and Engineering Hierarchical Supramolecular Framework for Enhanced Iodine Uptake

Ye Tao,^{‡a} Qiubing Dong,^{‡c} Jingmeng Wan,^b Fu-Ping Huang,^{*a} Jingui Duan,^{*b,d} and Ming-Hua Zeng^{*a}

^a State Key Laboratory for Chemistry and Molecular Engineering of Medicinal Resources, School of Chemistry & Pharmaceutical Sciences, Guangxi Normal University, Guilin 541004, China.

^b State Key Laboratory of Materials-Oriented Chemical Engineering, College of Chemical Engineering, Nanjing Tech University, Nanjing 211816, China.

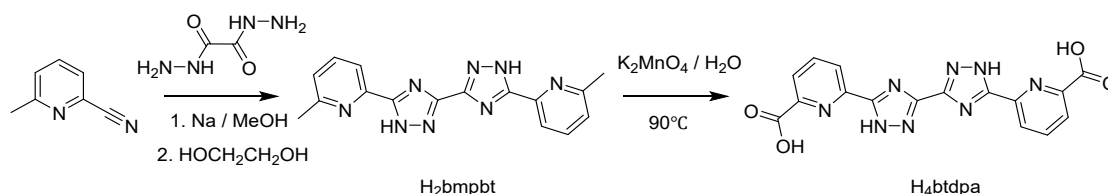
^c College of Chemistry and Materials Science, Anhui Normal University, Wuhu, Anhui 241000, China.

^d State Key Laboratory of Chemistry and Utilization of Carbon-Based Energy Resources, College of Chemistry, Xinjiang University, Urumqi, 830017, China.

General Information

Except for the ligands, the other chemicals were commercial products and were used without any further purification. The Fourier transform infrared data were obtained on a Perkin-Elmer Spectrum One FT-IR spectrometer. Powder X-ray diffraction was measured on a Rigaku D/max diffractometer equipped (Cu-K α , $\lambda = 1.54056 \text{ \AA}$). A FEI Quanta 200 scanning electron microscope (SEM) was used to determine the morphology. ESI-MS measurements were conducted on a Thermo Exactive instrument at a capillary temperature of 275 K. A liquid of the solution was injected into the device at 0.3 mL/h. The data were collected in negative ion mode. The spectrometer had previously been calibrated with a standard tune mix to give a precision of about 2 ppm in the region of m/z 300-2000; the tube lens voltage was set at 150 V and the skimmer voltage at 25 V. The in-source energy was set to a range of 0-100 eV with a gas flow rate at 10% of the maximum. The Raman spectral data were obtained on the inVia Quotation Raman spectrometer. UV-vis spectra were measured on a Shimadzu UV 2600 spectrometer.

General Procedure for ligand synthesis



Synthesis of H₂bmpbt. 2-Cyano-6-methylpyridine (5.4 g, 50.0 mmol) was dissolved in 70 mL of dry methanol with stirring at room temperature. Metallic sodium (0.2 g, 5 mmol) was added to the clear solution, followed by stirring at room temperature for 2 h. Oxalyl dihydrazide (3.0 g, 25.4 mmol) was then added to the solution, and the resulting white solid was refluxed for approximately 6 h. A bright yellow solid was obtained on cooling, isolated by suction filtration, and washed with methanol. Add the yellow solid mentioned above to 100 mL of ethylene glycol solution, heat, and reflux for about 5 hours, then cool slightly and pour it into water to precipitate a gray white solid. Wash the solid with water. Yield: 72%.

Synthesis of H₄btdpa. To a stirred aqueous solution (500 mL) of H₂bmpbt (6.4 g, 20 mmol) was added finely ground KMnO₄ (15.8 g, 100 mmol) over a period of 2 h, keeping the temperature of the mixture to 95 °C for 8 h, the precipitated MnO₂ was removed by filtration. Then the filtrate was concentrated to the 1/4 of original volume. Finally, when the pH value of the mixture was

adjusted to 4 by using 70% H₂SO₄, the target compound, as a white solid, was obtained by filtration and washed with water for three times. Yield: 52%.

Synthesis of 1: [Zn₉(btdpa)₃(EG)₆].5.5H₂O. A mixture of Zn(NO₃)₂·6H₂O (0.090 g, 0.3 mmol), 6,6'-(4H,4'H-[3,3'-bi(1,2,4-triazole)]-5,5'-diyl)dipicolinic acid (0.038 g, 0.1 mmol), ethylene glycol (EG, 1 mL) and DMF (7 mL) was stirred on a magnetic stirrer for 20 min. Then it was heated in a Teflon-lined stainless steel vessel (25 mL) at 160 °C for 5-72 h. The colourless rhombic block crystals of **1** were collected and washed with DMF (3 × 3 mL) and dried at air. Yield: 0.045 g (27%). IR data (KBr cm⁻¹): 3415(s), 3101(m), 2922(m), 1635(s), 1606(s), 1578(m), 1465(w), 1399(s), 1378(s), 1292(s), 1181(w), 1154(w), 1120(w), 1076(s), 1032(m), 1012(m), 891(m), 788(w), 756(s), 718(m), 675(w), 565(w), 510(w), 438(w).

SQUEEZE calculations: found 336 e⁻/f.u., calcd 330 e⁻/f.u. for 5.5 H₂O per f.u.

Synthesis of 2: [Zn₅₄(btdpa)₁₈(PDO)₁₈(HNMe₂)_{21.6}].16PDO·30DMF. A mixture of **1** (0.080 g, 4 mmol), 1,3-propanediol (PDO, 1 mL) and DMF (7 mL) was stirred on a magnetic stirrer for 20 min. Then it was heated in a Teflon-lined stainless steel vessel (25 mL) at 160 °C for 48 h. Colourless octahedral crystals of **2** were collected and washed with DMF (3 × 3 mL) and dried at air. Yield: 0.031g (35%). here protonated dimethylamine (HNMe₂) comes from the decomposition of DMF. In addition, **2** can also be synthesized directly. A mixture of Zn(NO₃)₂·6H₂O (0.090 g, 0.3 mmol), 6,6'-(4H,4'H-[3,3'-bi(1,2,4-triazole)]-5,5'-diyl)dipicolinic acid (0.038 g, 0.1 mmol), 1,3-propanediol (1mL) and DMF (7 mL) was stirred on a magnetic stirrer for 20 min. Then it was heated in a Teflon-lined stainless steel vessel (25 mL) at 160 °C for 24 h. Yield: (40%, based on H₄btdpa). IR data (KBr cm⁻¹): 3404(s), 2950(m), 1651(s), 1604(s), 1576(m), 1470(m), 1401(s), 1376(s), 1316(w), 1280 (m), 1179(w), 1148(w), 1074(m), 1027(m), 1012(m), 880(w), 848(w), 790(m), 755(m), 718(m), 672(w), 499(w), 432(w).

SQUEEZE calculations: found 1848 e⁻/f.u., calcd 1872 e⁻/f.u. for 30 DMF and 16 PDO per f.u.

Single crystal X-ray study. Single crystal X-ray diffraction data collection was conducted on an XtaLAB Synergy (Rigaku, Japan) diffractometer (Cu X-ray source, K α , λ = 1.54056 Å). The empirical absorption correction was based on equivalent reflections. The structure was solved by direct methods (SHELXL-2018 and Olex2) and refined by full-matrix least-squares refinements based on F^2 .^[1] Modeling of disordered end group atoms and iodine species in the structure through cleavage

disorder treatment. Anisotropic thermal parameters were applied to all non-hydrogen atoms. The hydrogen atoms were generated geometrically. Solvent molecules in the complexes were significantly disordered and could not be modeled properly due to the lack of well-defined atomic positions. Thus, the SQUEEZE procedure implemented in the PLATON^[2] software was employed to calculate the diffraction contribution of the solvent molecules and thereby produce a set of solvent-free diffraction intensities. Crystal data and structure refinement are summarized in Table S1. CCDC No. 2323878-2323880 for **1**, **2** and **I₂@2**, respectively.

Mass Spectrometry Measurements. Electrospray ionization mass (ESI-MS) spectrometry was recorded using a Thermo Exactive plus mass spectrometer, and the data were collected in negative ion mode. ESI-MS measurements were conducted at a capillary temperature of 275 °C. Aliquots of the solution were injected into the device at 0.3 mL/h. The spectrometer was previously calibrated with the standard tune mix to give a precision of ca. 2 ppm in the region of 300-4000 m/z. The capillary voltage was 50 V, the tube lens voltage was 150 V, and the skimmer voltage was 25 V. The in-source energy was set to 0 eV with a gas flow rate at 10% of the maximum.

Preprocessing: Dissolve 2 mg of fresh crystal **2** in 1 ml of DMSO. After sonication for 20 minutes, centrifuge the mixture (ensure slight dissolution). Take 100 µl of the supernatant and dilute it with chromatographically pure methanol to a final volume of 500 µl prior to use. For liquid samples, similarly take 100 µl of the centrifuged supernatant and dilute it with chromatographically pure methanol to a total volume of 500 µl before application.

Sample activation. Solvent-exchanged **1** and **2** crystals were prepared by immersing the as-synthesized samples in dry ethyl acetate for 3 days to remove the nonvolatile solvents, and the extract was decanted 3 times per day and fresh ethyl acetate was replaced. The completely activated sample was obtained by heating the solvent-exchanged sample at RT for 2 h and then 40°C for 12 h under a dynamic high vacuum.

Single-component gas adsorption. Single gas adsorption isotherms were measured on a Belsorp volumetric adsorption instrument (BEL Japan Corp.). In the measurements, ultra-high-purity grade gases of N₂, C₂H₄, C₂H₂, and CO₂ were used throughout the adsorption experiments.

Ideal adsorbed solution theory (IAST)^[3] was used to predict binary mixture adsorption as well as the separation factor from the experimentally obtained isotherms. In order to perform the integrations required by IAST, the single-component adsorption isotherms should be fitted by a

proper model. There is no restriction on the choice of the model to fit the adsorption isotherm, but data over the pressure range under study should be fitted very precisely. The dual-site Langmuir-Freundlich equation was used to fit the experimental data:

$$q = q_{m1} \cdot \frac{b_1 \cdot P^{1/n_1}}{1 + b_1 \cdot P^{1/n_1}} + q_{m2} \cdot \frac{b_2 \cdot P^{1/n_2}}{1 + b_2 \cdot P^{1/n_2}} \quad (1)$$

Here, P is the pressure of the bulk gas at equilibrium with the adsorbed phase (kPa), q is the adsorbed amount per mass of adsorbent (mol/kg), q_{m1} and q_{m2} are the saturation capacities of sites 1 and 2 (mol/kg), b_1 and b_2 are the affinity coefficients of sites 1 (1/kPa), and n_1 and n_2 represent the deviations from an ideal homogeneous surface.

Q_{st} calculation. Estimation of the adsorption heat was calculated by using Clausius- Clapeyron equation. Three different adsorption isotherms that were measured at different temperatures T_1 and T_2 are needed for the analysis. This software enables analysis with two or three adsorption isotherms. q_{st} at an adsorption amount can be calculated from the equation below with the difference between the 2 different pressures at the same adsorption amount (According to instruction of BEL master 7).

$$q_{st} = \frac{RT_1T_2}{T_2 - T_1} (\ln P_2 - \ln P_1)$$

Breakthrough measurements. The initial activated samples (1.265 g) were tightly packed into a stainless-steel column ($\varphi = 0.4$ cm, $L = 15$ cm), which was activated under vacuum at the corresponding temperature and then swept with He flow. Until no signal was detected by GC, the gas flow was dosed into the column. Breakpoints ($C_i/C_0 > 0.5\%$) were determined by gas chromatography. Between cycling experiments, re-generation was achieved under vacuum at 313 K for 2 h.

Table S1. Crystal data summary and structure refinement details, in which the formula contains estimated guests that have been treated by Squeeze.

Identification code	1	2	I ₂ @2
Formula	C ₆₀ H ₅₈ N ₂₄ O _{29.5} Zn ₉	C _{523.2} H _{705.2} N _{195.6} O ₁₇₀ Zn ₅₄	C ₃₄₈ H ₂₈₈ I _{56.6} N ₁₅₆ O _{118.8} Zn ₅₄
F. W.	2175.64	15985.07	19268.65
Crystal system	Trigonal	Cubic	Cubic
Temperature (K)	293(2)	100(1)	100(1)
Space group	<i>R-3c</i>	<i>Fd-3</i>	<i>Fd-3</i>
<i>a</i> (Å)	15.31573(19)	58.3017(2)	58.9792(3)
<i>b</i> (Å)	15.31573(19)	58.3017(2)	58.9792(3)
<i>c</i> (Å)	56.9773(7)	58.3017(2)	58.9792(3)
<i>a</i> (°)	90	90	90
<i>β</i> (°)	90	90	90
<i>γ</i> (°)	120	90	90
<i>V</i> (Å ³)	11574.6(3)	198173(2)	205162(3)
<i>Z</i>	6	8	8
<i>D_c</i> (g cm ⁻³)	1.874	1.072	1.248
<i>F</i> (000)	6558	65550	72306
Reflections	47231/3247	61406/14575	63826/16367
collected	<i>R</i> (int) = 0.0339	<i>R</i> (int) = 0.0253	<i>R</i> (int) = 0.0423
unique			
GOF on <i>F</i> ²	1.036	1.012	1.001
Final <i>R</i> indices	<i>R</i> ₁ = 0.0355,	<i>R</i> ₁ = 0.0390,	<i>R</i> ₁ = 0.0673,
<i>I</i> > 2σ(<i>I</i>)	ω <i>R</i> ₂ = 0.0976	ω <i>R</i> ₂ = 0.1259	ω <i>R</i> ₂ = 0.2138
<i>R</i> indices	<i>R</i> ₁ = 0.0420	<i>R</i> ₁ = 0.0434	<i>R</i> ₁ = 0.0865,
(all data)	ω <i>R</i> ₂ = 0.1030	ω <i>R</i> ₂ = 0.1288	ω <i>R</i> ₂ = 0.2341

$$R_1 = \sum ||F_o| - |F_c|| / \sum |F_o|; wR_2 = [\sum w(\sum F_o^2 - F_c^2)^2 / \sum w(F_o^2)^2]^{1/2}$$

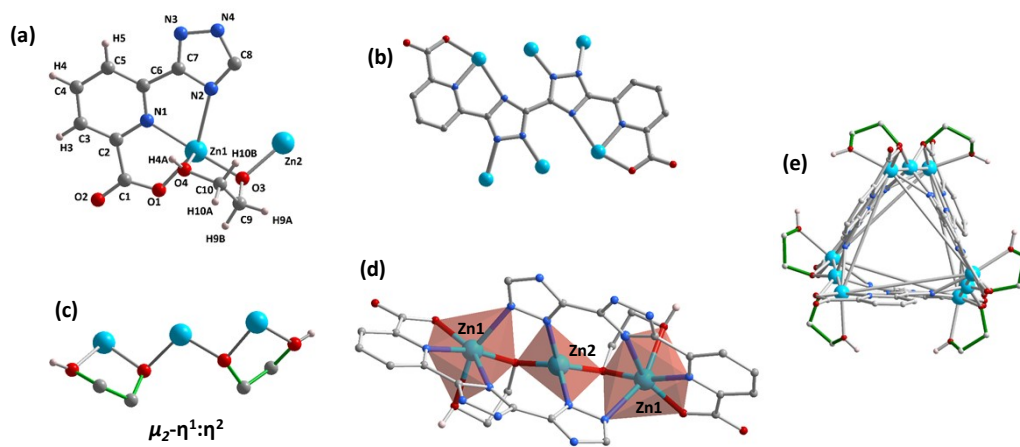
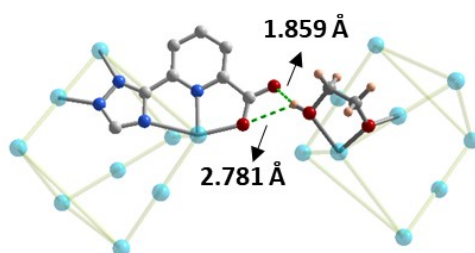


Fig. S1 Detailed structure of **1**: (a) View of the asymmetry unit; (b) ligand connection; (c) EG connection with the O atoms adopting $\mu_2\text{-}\eta^1,\eta^2$ code; (d) coordination mode of trimeric metal cluster; (e) two EG molecules coordinated with three Zn(II) in each edges of $[\text{Zn}_9]$ cluster.



Intermolecular H-bonding

Fig. S2 H-bonding interaction between the two adjacent $[\text{Zn}_9]$ clusters in **1**.

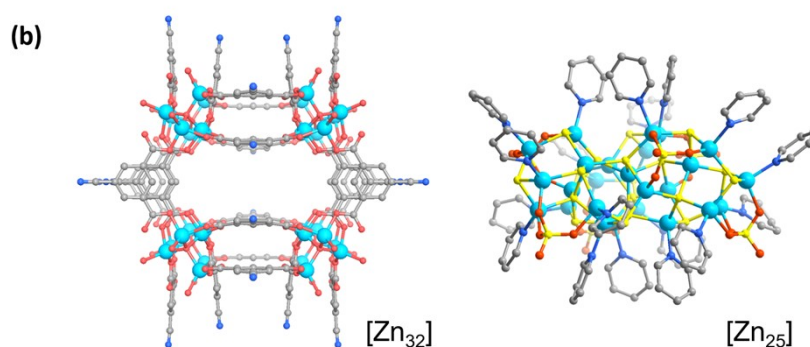
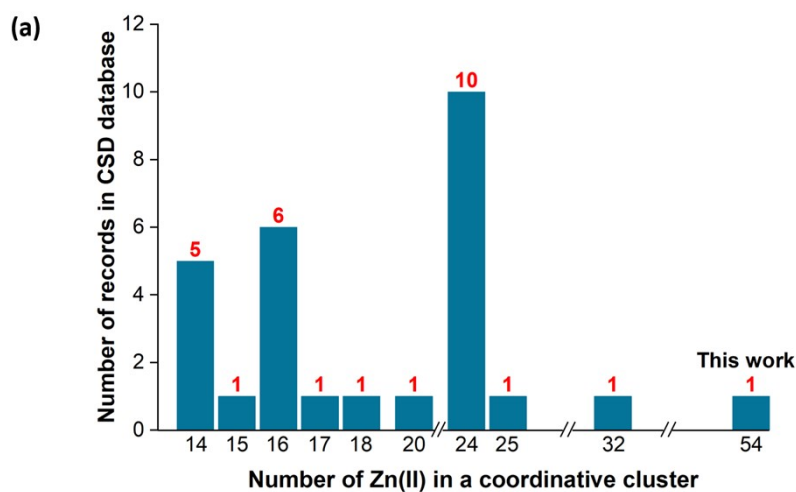


Fig. S3 (Up) Statistical chart of all known polynuclear coordinative clusters with Zn(II) numbers higher than 14, based on the Cambridge Structural Database (Version 5.45, till Mar 2024). (Down) Structure view of the two previous records of $[Zn_{32}]$ and $[Zn_{25}]$ with the highest Zn(II) numbers in the Cambridge Structural Database.

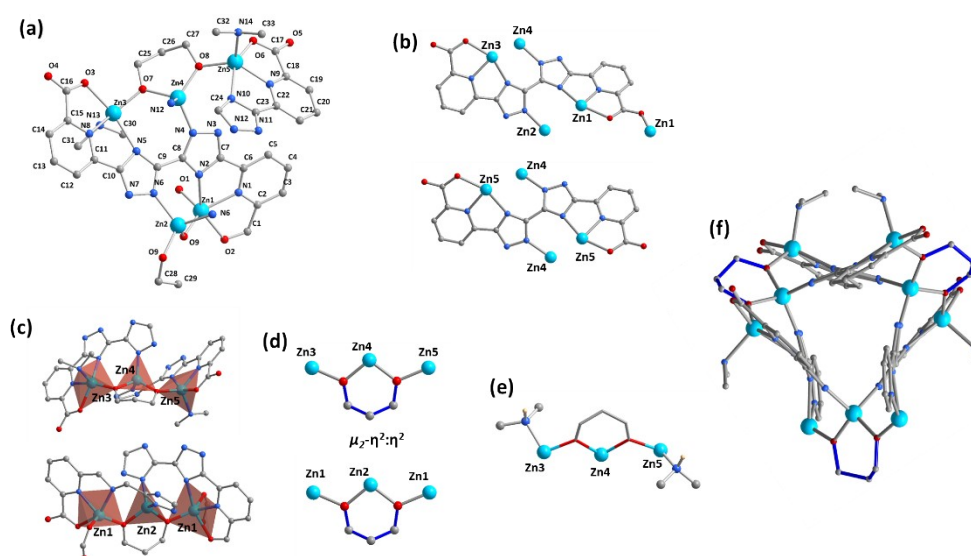


Fig. S4 Detailed structure of **2**: (a) asymmetry unit; (b) two types of ligand connection; (c) two types of trimeric metal cluster; (d) PDO connection with the O atoms adopting the $\mu_3\text{-}\eta^2\text{:}\eta^2$ mode; (e) $\text{HN}(\text{CH}_3)_2$ connection; (f) three PDO molecules in the distorted $[Zn_9]$ unit, different with the block in **1**.

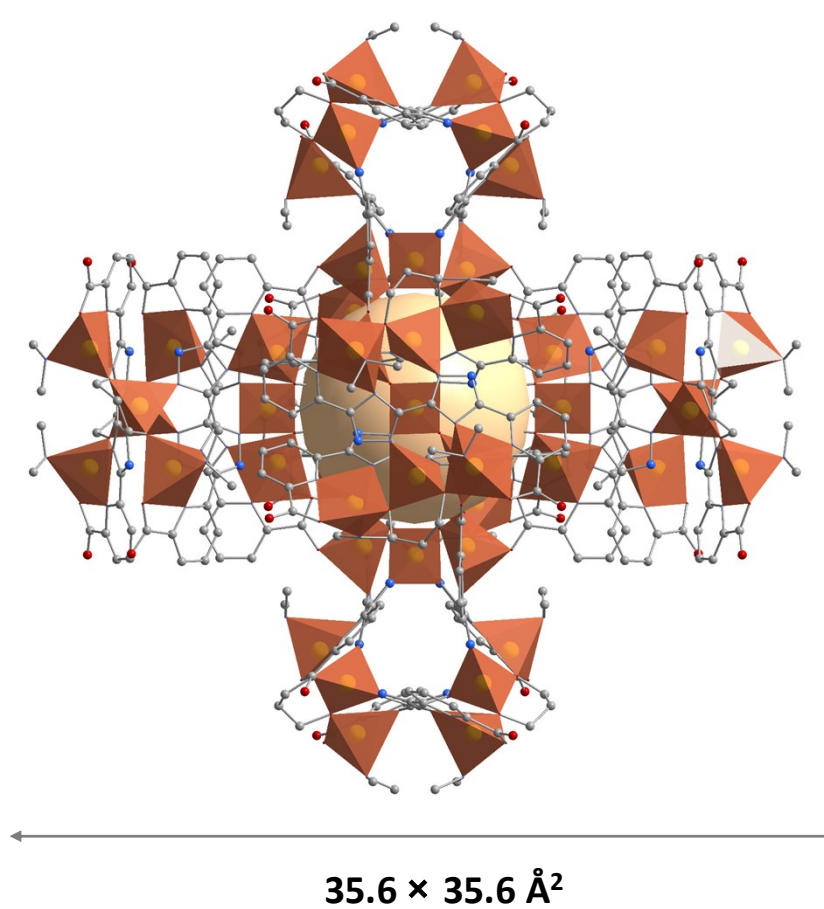


Fig. S5 Dimensions of the [Zn₅₄] cluster in **2**.

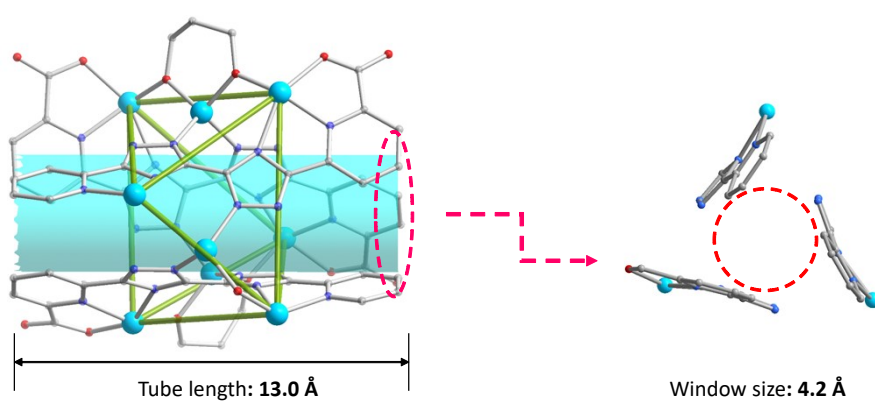


Fig. S6 Window size and tube length of pore A in **2**.

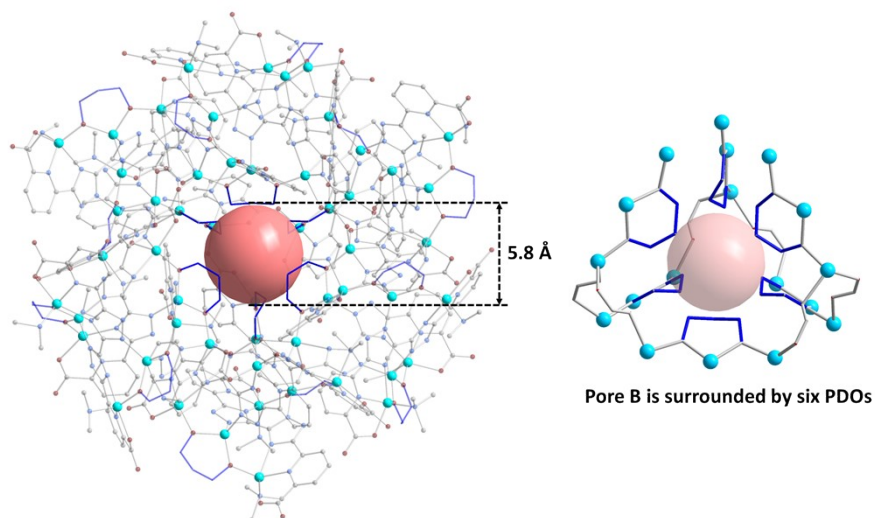


Fig. S7 Aperture size and its environment of the pore B in **2**. Color code: N, sky blue; PDO, dark blue.

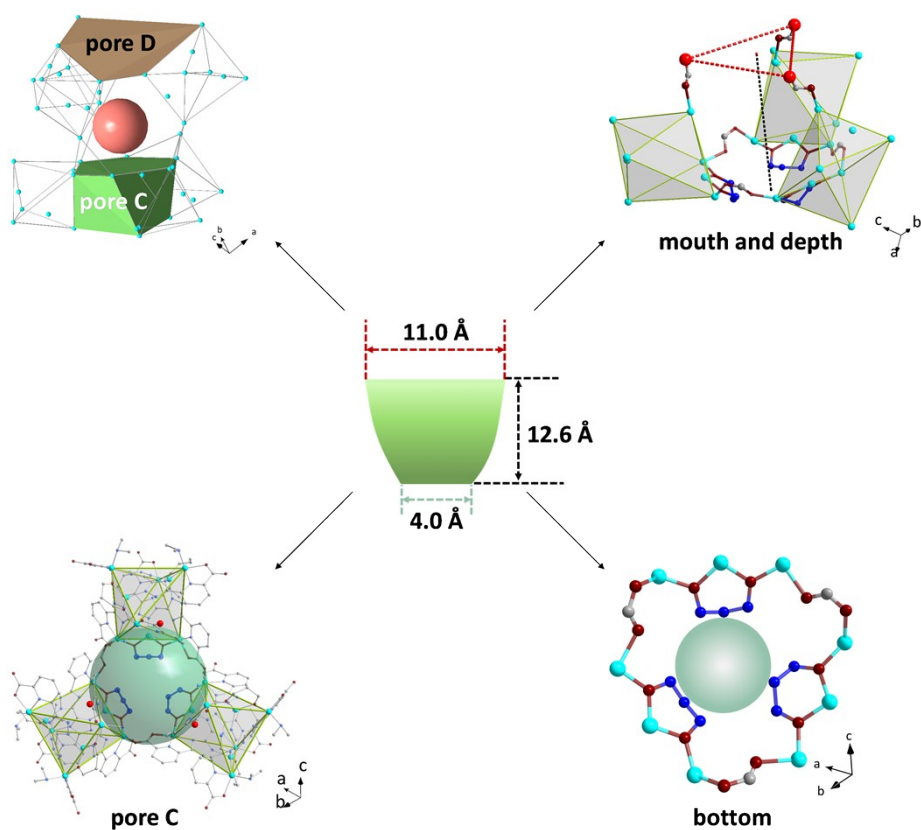


Fig. S8 Geometry of the bowl-shaped pore C in **2**. Color code: N, sky blue; PDO, dark blue.

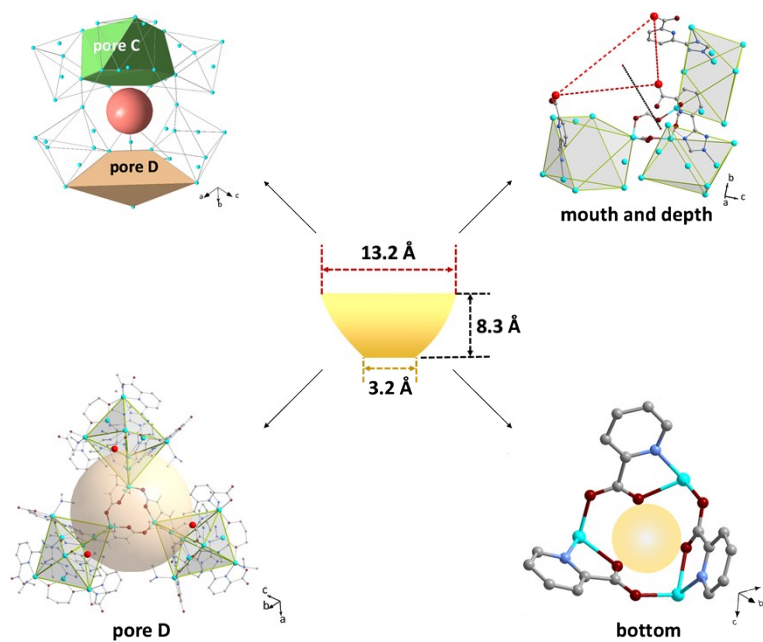


Fig. S9 Geometry of the bowl-shaped pore D in 2.

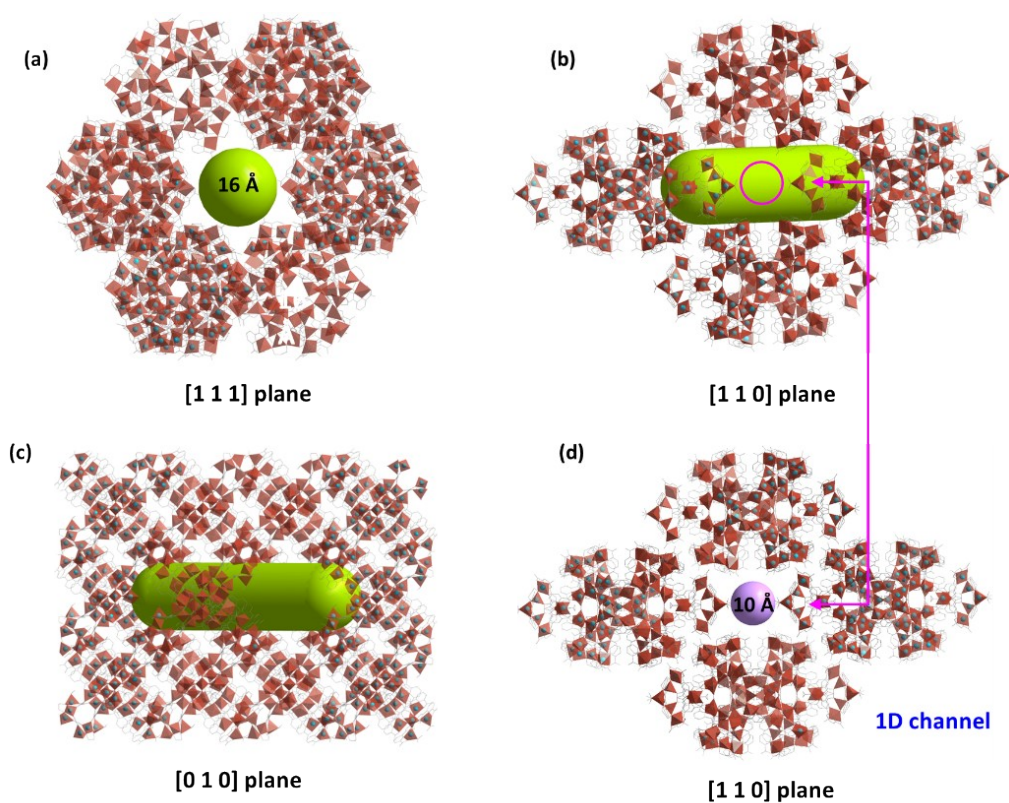


Fig. S10 (a-c) Pore E, viewed along $[1\ 1\ 1]$ plane (the cluster at center was omitted for clear), $[1\ 1\ 0]$ plane, and $[0\ 1\ 0]$ plane, respectively; (d) 1D channel, viewed along $[1\ 1\ 0]$ plane.

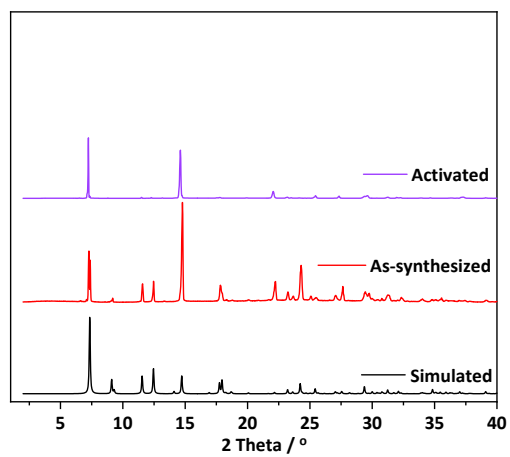


Fig. S11 PXR D patterns of 1.

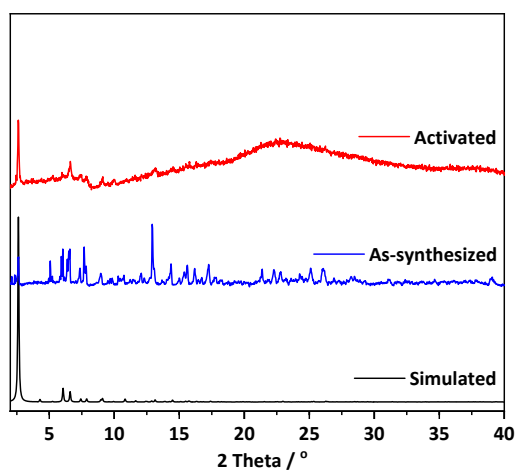


Fig. S12 PXR D patterns of 2.

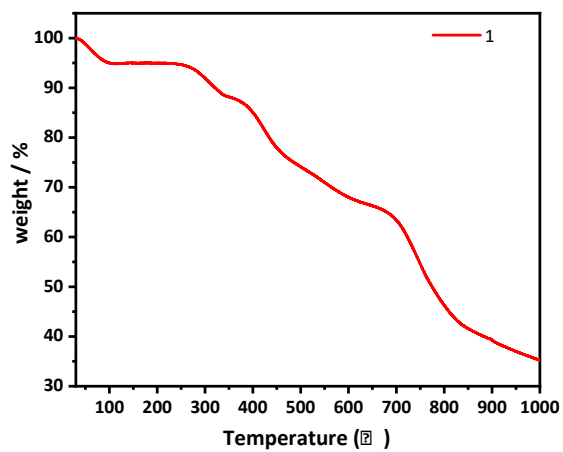


Fig. S13 Thermogravimetry analysis of 1.

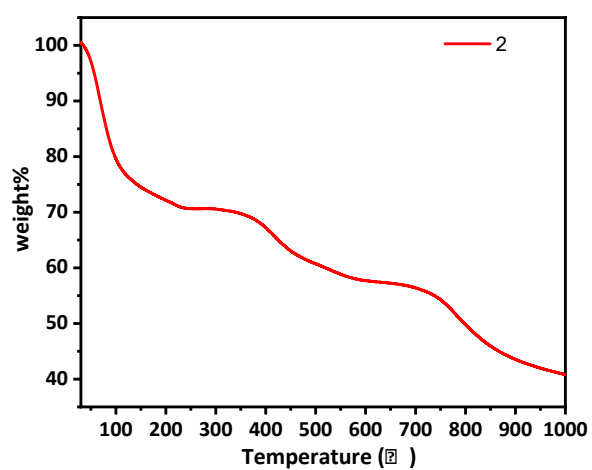


Fig. S14 Thermogravimetry analysis of 2.

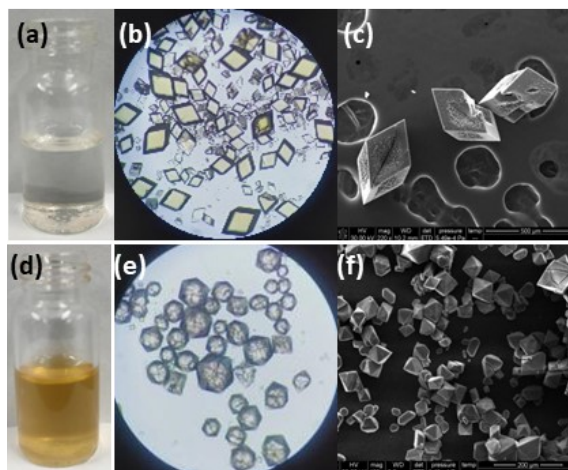


Fig. S15 Crystals morphology and SEM images of **1** (a,b,c) from **2** (d,e,f).

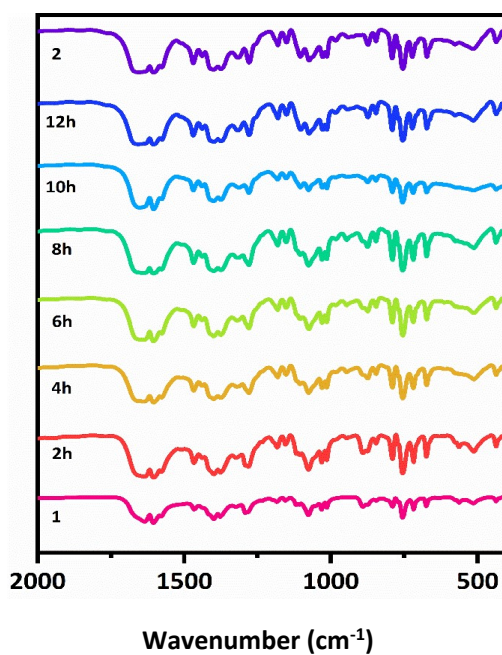


Fig. S16 IR spectroscopy of **1** and **2** and time-dependent IR spectroscopy for the conversion from **1** to **2**. No obvious spectroscopy change certifies the same type of covalent/coordinate bonds.

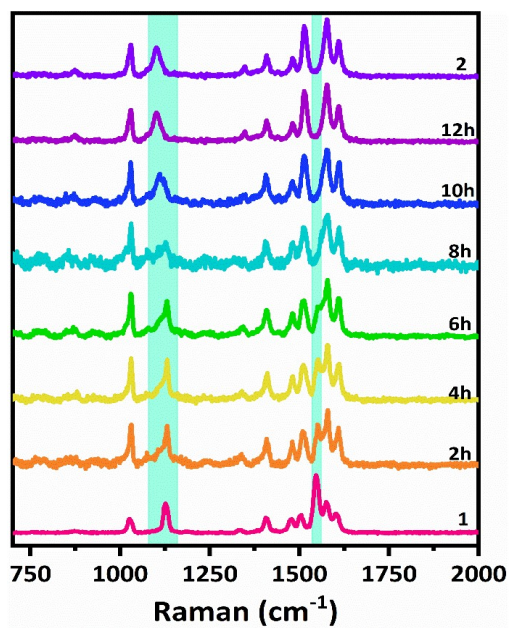


Fig. S17 Raman spectroscopy of **1** and **2** and time-dependent Raman spectroscopy for the reaction from **1** to **2**. The shift of the peaks, highlighted by cyan, indicates the structure change from **1** to **2**.

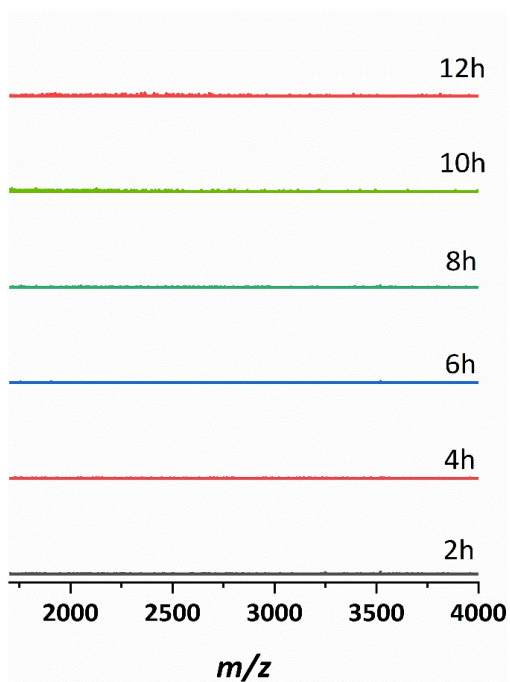


Fig. S18 ESI-MS ($m/z = 1400$ to 4000) spectra of the reaction solution from **1** to **2**.

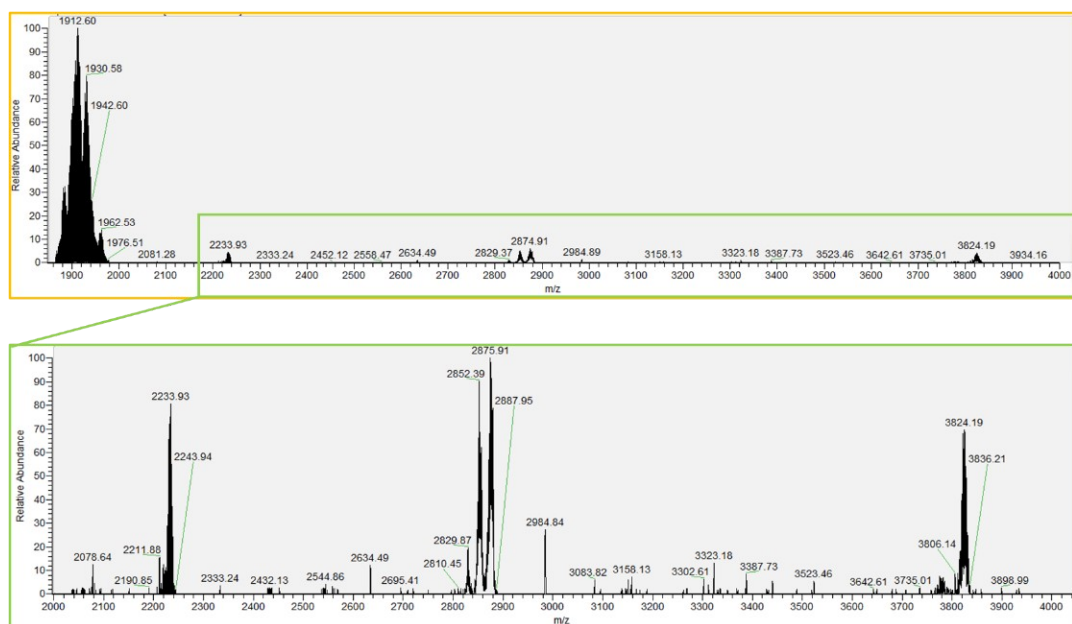


Fig. S19 ESI-MS spectra of **2** (negative mode).

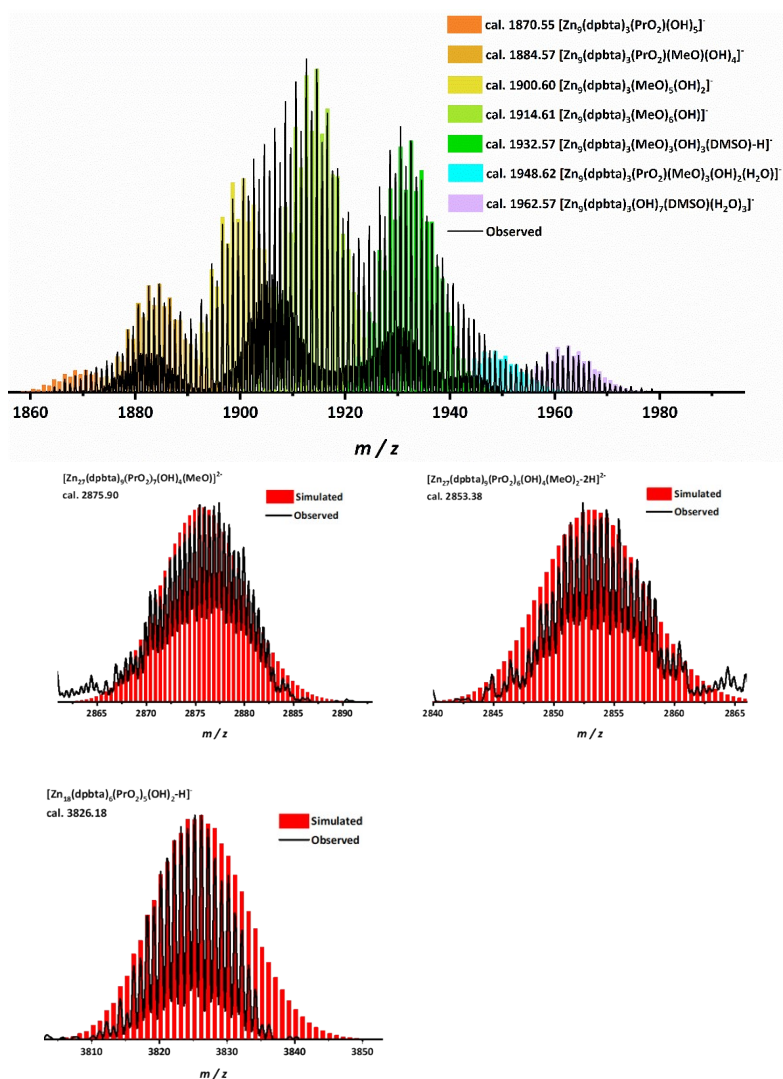


Fig. S20 The superposed simulated and observed spectra of ESI-MS species for **2** in negative mode.

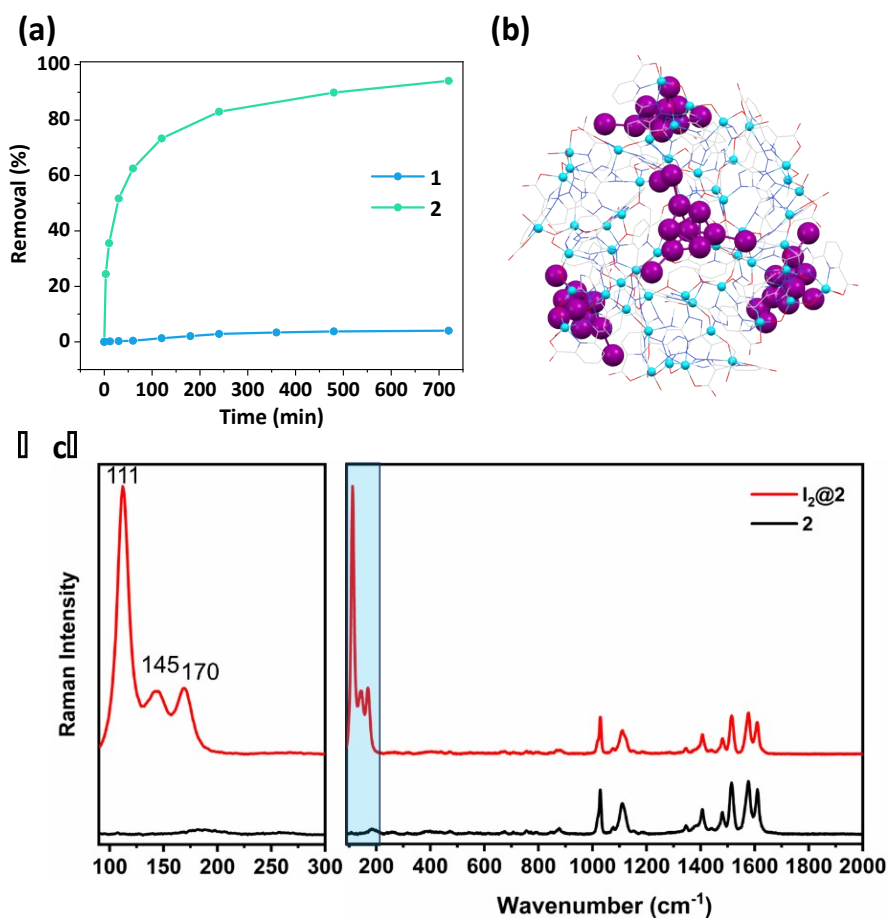


Fig. S21 Removal efficiency of I₂ for **1** and **2** in iodine/cyclohexane solution (a), disordered iodine species in **2** (b), the Raman spectra of **2** and I₂@**2** (c). The peak 111 and 145 can be attributed to the symmetric and asymmetric vibration of the I₃ anion, and the peak 170 is associated with "perturbed" iodine with charge-transfer complexes.

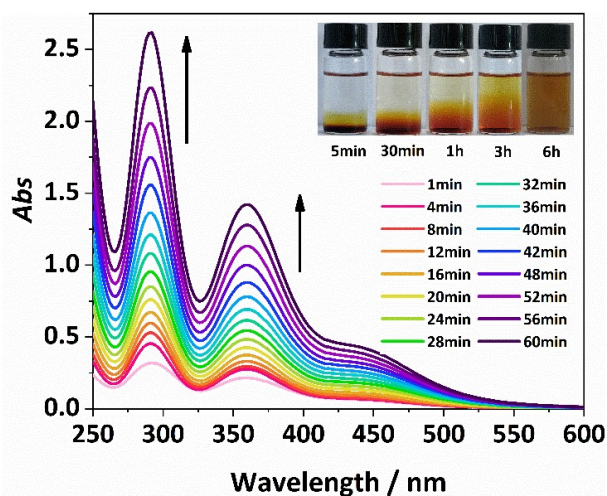


Fig. S22 Temporal evolution of absorbance for I₂-released process of I₂@**2** in EtOH. Inset: Photographs of iodine releasing process.

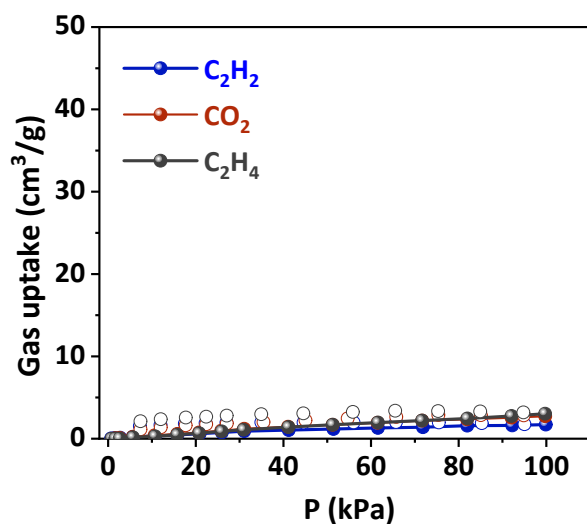


Fig. S23 C₂H₂, CO₂ and C₂H₄ adsorption isotherms of **1** at 298 K.

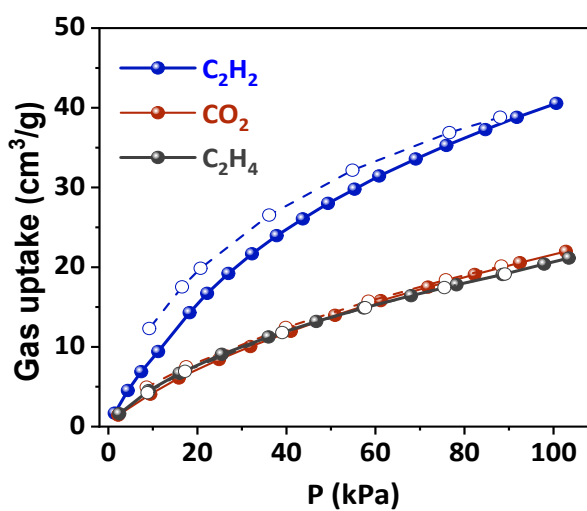


Fig. S24 C₂H₂, CO₂ and C₂H₄ adsorption isotherms of **2** at 298 K.

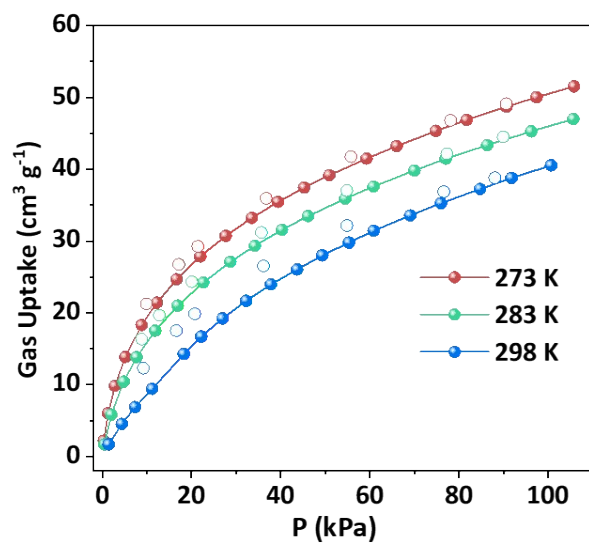


Fig. S25 C₂H₂ adsorption isotherms of **2** at 273, 283, 298 K.

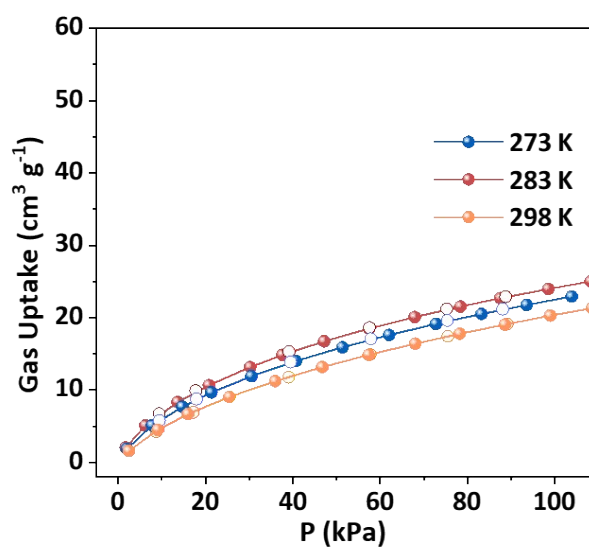


Fig. S26 C₂H₄ adsorption isotherms of **2** at 273, 283, 298 K.

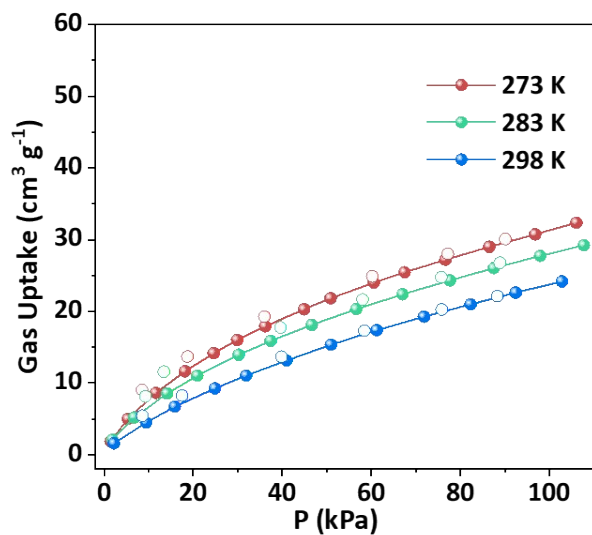


Fig. S27 CO₂ adsorption isotherms of **2** at 273, 283, 298 K.

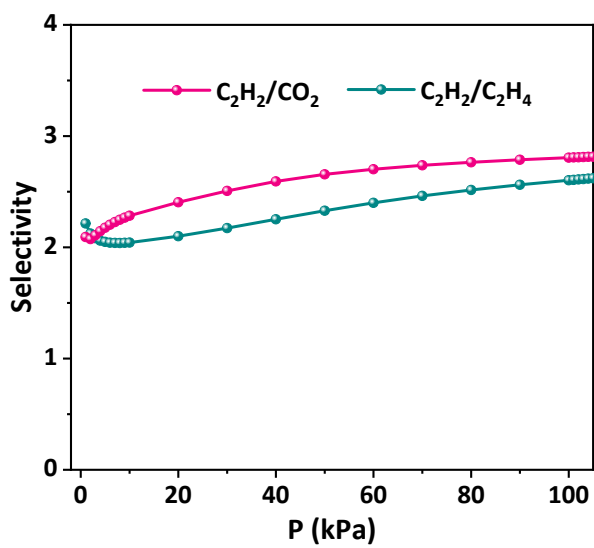


Fig. S28 IAST selectivities of C₂H₂/CO₂ (50/50) and C₂H₂/C₂H₄ (1/99) of **2** at 298 K, 1 bar.

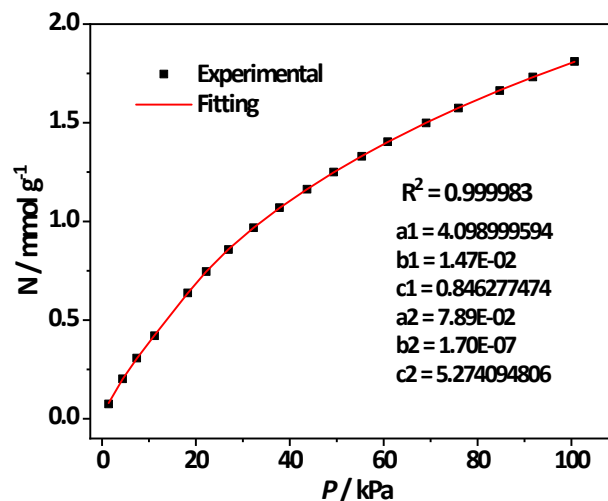


Fig. S29 DSLF fitting of the C_2H_2 sorption data for **2** at 298 K, 1 bar.

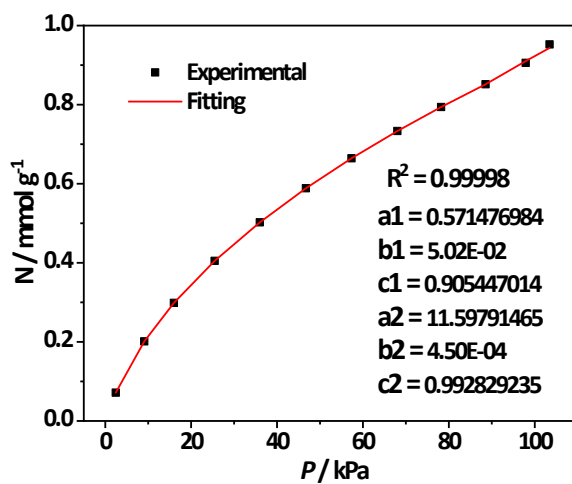


Fig. S30 DSLF fitting of the C_2H_4 sorption data for **2** at 298 K, 1 bar.

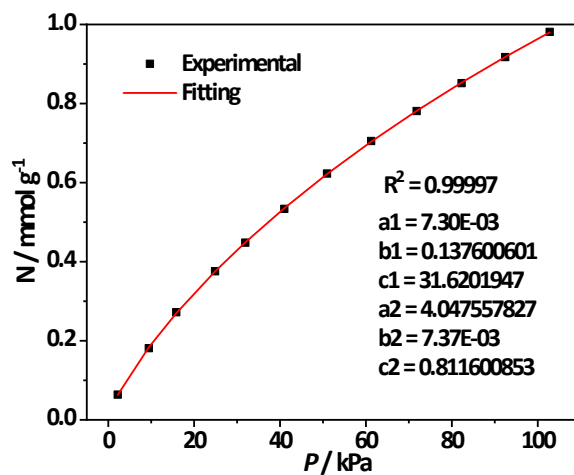


Fig. S31 DSLF fitting of the CO₂ sorption data for **2** at 298 K, 1 bar.

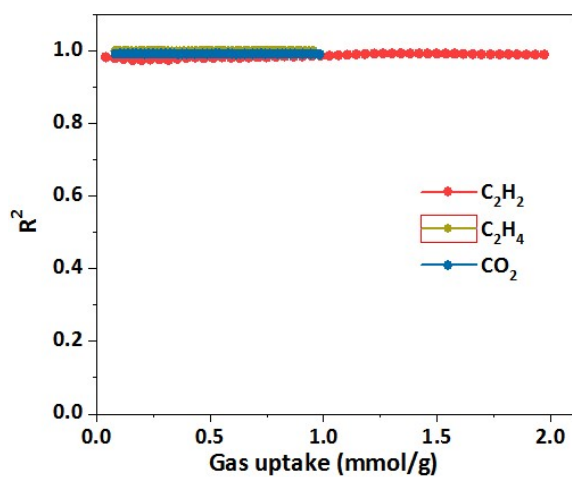


Fig. S32 The R^2 value for isotherms fitting with experimental data during adsorption heat calculation of **2**.

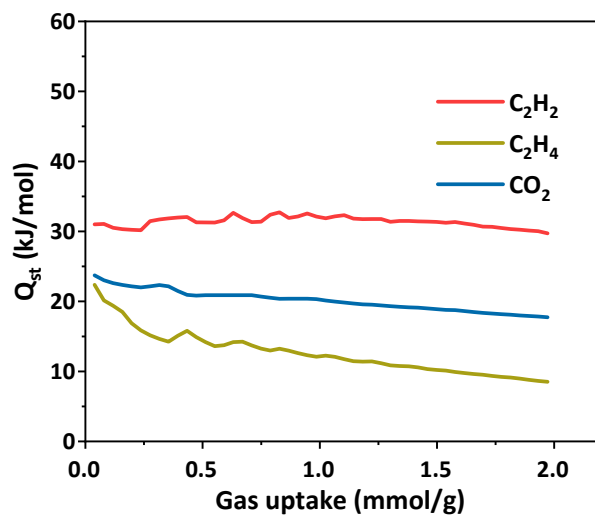


Fig. S33 Q_{st} of C_2H_2 , CO_2 and C_2H_4 of **2**.

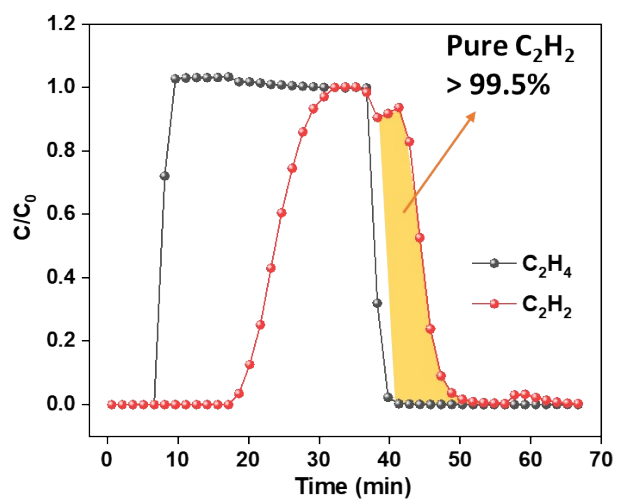


Fig. S34 Breakthrough curves of **2** for C_2H_2/C_2H_4 (v/v, 1/99) with desorption at 298 K, 1 bar.

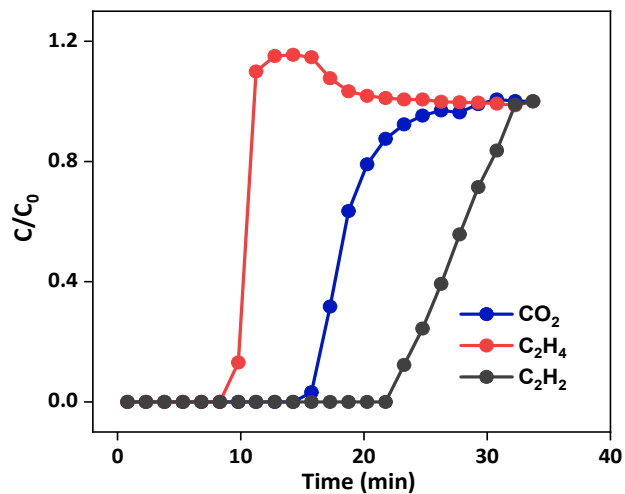


Fig. S35 Breakthrough result of 2 for C₂H₂/CO₂/C₂H₄ (v/v/v, 1/9/90) at 298 K, 1 bar.

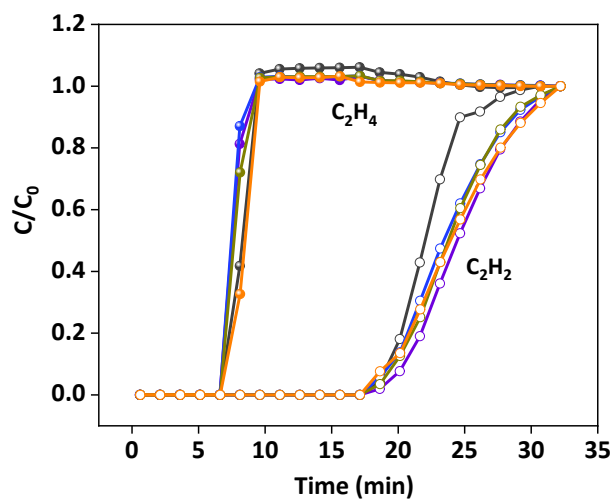


Fig. S36 Cycling breakthrough results of C₂H₂/C₂H₄ on 2 at 298 K, 1 bar.

Table S2 Selected bond length (Å) and bond angle (°) of complexes.

1. (A) $-y+1, x-y, z$; (B) $x-y+1/3, -y+2/3, -z+1/6$; (C) $-x+4/3, -x+y+2/3, -z+1/6$.			
Atomic Distances [Å]			
Zn1—O1	2.066 (2)	Zn1—N3A	2.325 (2)
Zn1—O3	1.9341 (18)	Zn2—O3	1.9068 (18)
Zn1—O4	2.213 (3)	Zn2—O3B	1.9066 (18)
Zn1—N1	2.033 (2)	Zn2—N4C	1.991 (2)
Zn1—N2	2.515 (2)	Zn2—N4A	1.991 (2)
Bond Angles [°]			
O1—Zn1—O4	94.49 (10)	N1—Zn1—O4	89.92 (9)
O1—Zn1—N2	152.84 (8)	N1—Zn1—N2	73.41 (8)
O1—Zn1—N3A	106.58 (9)	N1—Zn1—N3A	100.87 (8)
O3—Zn1—O1	106.62 (8)	N3A—Zn1—N2	81.21 (7)
O3—Zn1—O4	79.77 (9)	O3—Zn2—O3B	110.06 (11)
O3—Zn1—N1	168.29 (9)	O3—Zn2—N4A	98.01 (8)
O3—Zn1—N2	99.63 (7)	O3—Zn2—N4C	125.16 (8)
O3—Zn1—N3A	87.08 (8)	O3B—Zn2—N4C	98.02 (8)
O4—Zn1—N2	83.29 (9)	O3B—Zn2—N4A	125.17 (9)
O4—Zn1—N3A	157.68 (9)	N4A—Zn2—N4C	102.77 (12)
N1—Zn1—O1	79.54 (8)		
2. (A) $y, -z+5/4, -x+5/4$; (B) $-x+5/4, y, -z+5/4$; (C) $-z+5/4, x, -y+5/4$.			
Atomic Distances [Å]			
Zn1—O1A	1.9903 (16)	Zn3—N8	2.043 (2)
Zn1—O2	2.1658 (16)	Zn3—N13	2.081 (2)
Zn1—O9B	1.9087 (15)	Zn4—O7	1.9323 (17)
Zn1—N1	2.0585 (18)	Zn4—O8	1.9286 (19)
Zn1—N2	2.2736 (18)	Zn4—N4	2.0017 (19)
Zn2—O9	1.9231 (15)	Zn4—N12B	2.005 (2)
Zn2—O9B	1.9232 (15)	Zn5—O6	2.131 (3)
Zn2—N6B	1.9926 (18)	Zn5—O8	1.915 (2)
Zn2—N6	1.9925 (18)	Zn5—N9	2.051 (3)
Zn3—O3	2.1353 (17)	Zn5—N10	2.300 (2)
Zn3—O7	1.9081 (19)	Zn5—N14	2.011 (5)
Zn3—N5	2.2213 (18)		
Bond Angles [°]			
O1A—Zn1—O2	105.58 (6)	N8—Zn3—O3	76.63 (7)
O1A—Zn1—N1	101.52 (7)	N8—Zn3—N5	76.06 (7)
O1A—Zn1—N2	88.65 (6)	N8—Zn3—N13	105.65 (9)
O2—Zn1—N2	150.20 (6)	N13—Zn3—O3	104.34 (8)
O9B—Zn1—O1A	120.47 (7)	N13—Zn3—N5	95.72 (8)
O9B—Zn1—O2	97.93 (6)	O7—Zn4—N4	111.83 (8)
O9B—Zn1—N1	137.34 (7)	O7—Zn4—N12B	105.06 (8)
O9B—Zn1—N2	96.94 (6)	O8—Zn4—O7	101.35 (8)
N1—Zn1—O2	76.08 (6)	O8—Zn4—N4	112.57(8)
N1—Zn1—N2	75.47 (7)	O8—Zn4—N12B	117.14 (9)
O9B—Zn2—O9	102.92 (9)	N4—Zn4—N12B	108.47 (8)
O9B—Zn2—N6B	112.85 (7)	O6—Zn5—N10	152.81 (12)
O9—Zn2—N6B	111.42 (7)	O8—Zn5—O6	100.17 (11)
O9—Zn2—N6	112.85 (7)	O8—Zn5—N9	130.83 (10)
O9B—Zn2—N6	111.42 (7)	O8—Zn5—N10	92.88 (8)
N6B—Zn2—N6	105.59 (10)	O8—Zn5—N14	112.97 (17)
O3—Zn3—N5	149.57 (7)	N9—Zn5—O6	77.92 (12)
O7—Zn3—O3	98.08 (8)	N9—Zn5—N10	75.51 (10)

Continued

O7—Zn3—N5	99.83 (7)	N14—Zn5—O6	97.80 (18)
O7—Zn3—N8	152.24 (9)	N14—Zn5—N9	115.96 (17)
O7—Zn3—N13	102.07 (9)	N14—Zn5—N10	98.88 (15)

I₂@2. (A) y, -z+5/4, -x+5/4; (B) -x+5/4, y, -z+5/4; (C) -z+5/4, x, -y+5/4.

Atomic Distances [Å]

Zn1—O1A	1.993 (3)	Zn4—O8	1.933 (3)
Zn1—O2	2.152 (3)	Zn4—O9	1.921 (4)
Zn1—O7	1.909 (3)	Zn4—N4	2.002 (3)
Zn1—N1	2.060 (3)	Zn4—C24	1.987 (5)
Zn1—N2	2.279 (3)	Zn5—O5	2.054 (16)
Zn2—O7B	1.934 (3)	Zn5—O5'	2.356 (17)
Zn2—O7	1.934 (3)	Zn5—O9B	1.888 (5)
Zn2—N6	1.998 (3)	Zn5—O10	2.183 (8)
Zn2—N6B	1.998 (3)	Zn5—N9	2.087 (7)
Zn3—O3	2.144 (3)	Zn5—N11	2.262 (5)
Zn3—O8	1.913 (4)	I1—I2	2.569 (10)
Zn3—N5	2.232 (3)	I1—I2'	2.669 (9)
Zn3—N8	2.046 (4)	I2—I3	2.889 (18)
Zn3—N13	2.057 (5)	I2—I3'	2.738 (19)

Bond Angles [°]

O1A—Zn1—O2	106.74 (11)	N13—Zn3—O3	101.08 (18)
O1A—Zn1—N1	102.38 (12)	N13—Zn3—N5	95.88 (16)
O1A—Zn1—N2	88.47 (11)	O8—Zn4—N4	113.76 (15)
O2—Zn1—N2	150.63 (10)	O8—Zn4—C24	104.47 (17)
O7—Zn1—O1A	119.57 (12)	O9—Zn4—O8	104.36(17)
O7—Zn1—O2	97.89 (10)	O9—Zn4—N4	109.07 (18)
O7—Zn1—N1	137.11 (12)	O9—Zn4—C24	117.3 (2)
O7—Zn1—N2	95.91 (11)	C24—Zn4—N4	108.00 (16)
N1—Zn1—O2	76.76 (11)	O5—Zn5—O10	88.9 (6)
N1—Zn1—N2	75.48 (12)	O5—Zn5—N9	79.9 (5)
O7—Zn2—O7B	101.62 (15)	O5—Zn5—N11	155.2 (5)
O7—Zn2—N6	111.67 (12)	O9B—Zn5—O5	104.4 (5)
O7—Zn2—N6B	112.82 (11)	O9B—Zn5—O10	111.3 (3)
O7B—Zn2—N6	111.67 (12)	O9B—Zn5—N9	135.2 (3)
O7B—Zn2—N6B	112.82 (11)	O9B—Zn5—N11	95.76 (18)
N6—Zn2—N6B	106.40 (18)	O9B—Zn5—O5'	95.6 (4)
O3—Zn3—N5	150.83 (14)	O10—Zn5—N11	97.2 (3)
O8—Zn3—O3	98.51 (15)	O10—Zn5—O5'	108.0 (5)
O8—Zn3—N5	100.44 (13)	N9—Zn5—O10	113.3 (3)
O8—Zn3—N8	152.21 (16)	N9—Zn5—N11	75.6 (2)
O8—Zn3—N13	103.35 (18)	N9—Zn5—O5'	74.3 (5)
N8—Zn3—O3	76.21 (14)	N11—Zn5—O5'	146.2 (4)
N8—Zn3—N5	76.67 (13)	I1—I2—I3	171.8(5)
N8—Zn3—N13	104.44 (17)		

Table S3 SHAPE analysis of the Zn^{II} ions in **1** and **2**.

Complex	Structure [ML5]	PP-5	vOC-5	TBPY-5	SPY-5	JTBPY-5
1	Zn1	30.794	3.742	3.202	2.231	4.581
	Zn3	27.715	2.569	5.366	1.377	7.028
	Zn5	29.593	4.706	2.441	2.755	3.947
	Structure [ML4]	SP-4	T-4	SS-4	vTBPY-4	
	Zn2	30.750	0.249	8.834	3.460	-
	Zn4	29.281	0.429	7.653	2.493	-
2	Structure [ML6]	HP-6	PPY-6	OC-6	TPR-6	JPPY-6
	Zn1	32.991	22.230	3.097	11.127	25.785
	Structure [ML4]	SP-4	T-4	SS-4	vTBPY-4	
	Zn2	21.298	2.064	6.017	5.275	

SPY-5 4 C_{4v} Spherical square pyramid TBPY-5 3 D_{3h} Trigonal bipyramid
 OC-6 3 O_h Octahedron T-4 2 T_d Tetrahedron

Table S4 The dihedral angle presented inside the ligand in the structures.

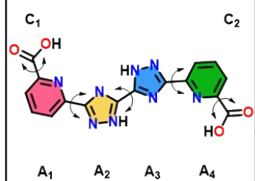
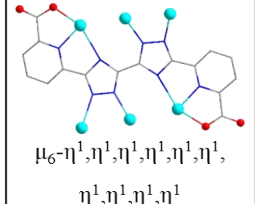
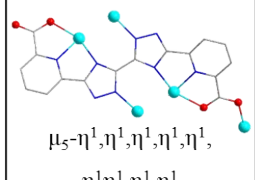
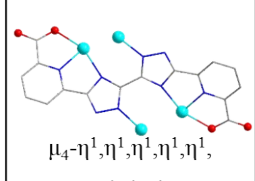
Co md.		Dihedral angles(°)							
		C ₁ A ₁	A ₁ A ₂	A ₂ A ₃	A ₃ A ₄	C ₂ A ₄	A ₁ A ₃	A ₁ A ₄	A ₂ A ₄
1	 $\mu_6\text{-}\eta^1, \eta^1, \eta^1, \eta^1, \eta^1, \eta^1,$ $\eta^1, \eta^1, \eta^1, \eta^1$	2.7	8.0	9.7	8.0	2.7	8.7	13.5	8.7
2	 $\mu_5\text{-}\eta^1, \eta^1, \eta^1, \eta^1, \eta^1,$ $\eta^1, \eta^1, \eta^1, \eta^1$	6.1	7.8	27.5	10.1	3.5	37.5	44.0	33.8
	 $\mu_4\text{-}\eta^1, \eta^1, \eta^1, \eta^1, \eta^1,$ η^1, η^1, η^1	2.8	9.2	35.8	9.2	2.8	44.3	53.1	44.3

Table S5 Diagram of internal dihedral angles of ligands in the structure.

Compound and ligand coordination patterns		The Angle (°) between carboxylic acid (C) and aromatic ring (A) and adjacent aromatic ring is shown as a comparison diagram				
		C ₁ A ₁	A ₁ A ₂	A ₂ A ₃	A ₃ A ₄	C ₂ A ₄
1	μ ₆ -η ¹ , η ¹ ,η ¹ ,η ¹ ,η ¹ ,η ¹ , η ¹ ,η ¹ ,η ¹ ,η ¹				-	-
	μ ₅ -η ¹ , η ¹ ,η ¹ ,η ¹ ,η ¹ , η ¹ ,η ¹ ,η ¹ ,η ¹					
2	μ ₄ -η ¹ , η ¹ ,η ¹ ,η ¹ ,η ¹ , η ¹ ,η ¹ ,η ¹				-	-

Table S6 Iodine adsorption capacities of various porous adsorbents.

Adsorbent	Category	Test conditions	Iodine loading capacity(g/g)	Refs.
2	MOC	Vapor adsorption, 75°C	3.19	This work
MOC-DASD	MOC-extended amorphous network	Vapor adsorption, 80°C	3.67	[4]
AIOC-162-C	MOC	Vapor adsorption, 80°C	2.35	[5]
Cage-1	MOC	Vapor adsorption, 75°C	1.42	[6]
MOC-19	MOC	Vapor adsorption, 25°C	0.5	[7]
Co-NDC	Clusters	Vapor adsorption, 25°C	0.346	[8]
Co-NDC-Br			0.452	
AIOC-26	Clusters	Vapor adsorption, 80°C	0.701	[9]
AIOC-27			0.503	
[Ti ₁₂ Pb ₅]	Cluster based layers	Vapor adsorption, 60°C	2.246	[10]
PCN-333-Al	MOF	Vapor adsorption, 75°C	4.420	[11]
UPC-158-HCl	MOF	Vapor adsorption, 70°C	2.920	[12]
[Zr ₆ O ₄ (OH) ₄ (L ⁷) ₆]	MOF	Vapor adsorption, 25°C	2.790	[13]
MOF-808	MOF	Vapor adsorption, 80°C	2.180	[14]
MFM-300(Sc)	MOF	Vapor adsorption, 70°C	1.540	[15]
ZIF-8	MOF	Vapor adsorption, 77°C	1.250	[16]
DUT-68(Zr)	MOF	Vapor adsorption, 80°C	1.081	[17]
JNU-200	MOF	Vapor adsorption, 80°C	1.08	[18]

References

- [1] a) G. M. Sheldrick, *Acta Cryst.* 2008, **64**, 112-122; b) O. V. Dolomanov, L. J. Bourhis, R. J. Gildea, J. A. K. Howard, and H. Puschmann, *J. Appl. Crystallogr.* 2009, **42**, 339-341.
- [2] A. Spek, *Acta Crystallogr. D* 2009, **65**, 148-155.
- [3] a) Y. S. Bae, K. L. Mulfort, H. Frost, P. Ryan, S. Punnathanam, L. J. Broadbelt, J. T. Hupp, and R. Q. Snurr, *Langmuir* 2008, **24**, 8592-8598; b) N. F. Cessford, N. A. Seaton, T. Düren, *Ind. Eng. Chem. Res.* 2012, **51**, 4911-4921.
- [4] S.-N. Liu, H.-N. Wang, M.-L. Feng, K.-L. Yang, S. Cai, J. Fan, W.-G. Zhang, and S.-R. Zheng, *ACS Appl. Nano Mater.* 2022, **6**, 656-663.
- [5] N. Yang, S. T. Wang, C. S. Li, J. Zhang, M. Y. Zhang, and W. H. Fang, *Small* 2024, **2311083**.
- [6] W.-Y. Pei, J. Yang, H. Wu, W. Zhou, Y.-W. Yang, and J.-F. Ma, *Chem. Commun.* 2020, **56**, 2491-2494.
- [7] W. Q. Xu, Y. H. Li, H. P. Wang, J. J. Jiang, D. Fenske, and C. Y. Su, *Chem. Asian. J.* 2015, **11**, 216-220.
- [8] J.-Y. Liu, T.-P. Sheng, C. Li, Z. Wang, F.-R. Dai, and Z.-N. Chen, *Cryst. Growth Des.* 2022, **22**, 3182-3189.
- [9] S. Yao, W.-H. Fang, Y. Sun, S.-T. Wang, and J. Zhang, *J. Am. Chem. Soc.* 2021, **143**, 2325-2330.
- [10] A. Said, C. Gao, C. Liu, H. Niu, D. Wang, Y. Liu, L. Du, and C.-H. Tung, Y. Wang, *Inorg. Chem.* 2021, **61**, 586-596.
- [11] Y. Tang, H. Huang, J. Li, W. Xue, and C. Zhong, *J. Mater. Chem. A* 2019, **7**, 18324-18329.
- [12] B. Guo, F. Li, C. Wang, L. Zhang, and D. Sun, *J. Mater. Chem. A* 2019, **7**, 13173-13179.
- [13] Marshall, R. J.; Griffin, S. L.; Wilson C.; and Forgan, R. S. *Chem. Eur. J.* 2016, **22**, 4870-4877.
- [14] P. Chen, X. He, M. Pang, X. Dong, S. Zhao, and W. Zhang, *ACS Appl. Mater. Interface* 2020, **12**, 20429-20439.
- [15] X. Zhang, I. da Silva, H. G. W. Godfrey, S. K. Callear, S. A. Sapchenko, Y. Cheng, I. Vitórica-Yrezábal, M. D. Frogley, G. Cinque, C. C. Tang, C. Giacobbe, C. Dejoie, S. Rudić, A. J. Ramirez-Cuesta, M. A. Denecke, S. Yang, and M. Schröder, *J. Am. Chem. Soc.* 2017, **139**, 16289-16296.
- [16] D. F. Sava, M. A. Rodriguez, K. W. Chapman, P. J. Chupas, J. A. Greathouse, P. S. Crozier and T. M. Nenoff, *J. Am. Chem. Soc.* 2011, **133**, 12398-12401.
- [17] L. Wang, T. Li, X. Dong, M. Pang, S. Xiao, and W. Zhang, *Chem. Eng. J.* 2021, **425**, 130578.
- [18] K. Wu, Y.-L. Huang, J. Zheng, D. Luo, M. Xie, Y. Y. Li, W. Lu, and D. Li, *Mater. Chem. Front.* 2021, **5**, 4300-4309.